Received: 7 August 2020 | Revised: 11 September 2020 | Accepted: 23 September 2020

DOI: 10.1002/nano.202000102

nano select Open Access WILEY

RESEARCH ARTICLE

Nanoparticle ink-based silicon Schottky diodes operating up to 2.84 GHz

Laura Kühnel[1] | **Kevin Neumann**[2] | **Julian Neises**[1] | **Fabian Langer**[1] | **Daniel Erni**[2] | **Roland Schmechel**[1] | **Niels Benson**[1]

[1] Institute of Technology for Nanostructures (NST), University of Duisburg-Essen, and CENIDE, Duisburg D-47048, Germany

[2] General and Theoretical Electrical Engineering (ATE), University of Duisburg-Essen, and CENIDE, Duisburg D-47048, Germany

Correspondence
Laura Kühnel and Niels Benson, Institute of Technology for Nanostructures (NST), University of Duisburg-Essen, and CENIDE, D-47048 Duisburg, Germany.
Email: laura.kuehnel@uni-due.de (L. K.); niels.benson@uni-due.de (N. B.)

Today's printed, flexible electronics are often limited by the electronic performance enabled by the used functional semiconductor ink. Thin films from such inks typically exhibit a low charge carrier mobility, which inhibits high frequency device operation and limits their use for applications within the Internet-of-Things concept, such as wireless electronic tags and sensors. Our approach to overcome this issue is the use of printable silicon. The silicon is deposited using nanoparticle inks and is subsequently processed into self-organized crystalline μ-cone shaped structures using an excimer laser treatment. Due to the high crystallinity of the Si μ-cones, they can be used for devices capable of high frequency operation. In this article, this is demonstrated on the example of a Schottky diode operating at switching speeds up to 2.84 GHz and thereby putting printable high frequency electronics within reach.

KEYWORDS
RFID tags, Schottky diode, semiconductor inks, silicon nanoparticle, UHF

1 | INTRODUCTION

As part of the Internet-of-Things (IoT) concept, where wireless communication and networking are of significant importance, the operational frequency of many targeted radio frequency identification (RFID) applications is located in the ultra-high-frequency (UHF) band (300 MHz to 3 GHz) or even higher. Potential applications include the full traceability and monitoring of "things", covering, for example, the sectors logistics (warehouse inventory, transportation of goods), security (anti-counterfeiting), and healthcare (wearable monitoring devices). One electronic key element for such applications is the diode. This versatile device can be used, for example, in energy harvesting circuits to extract energy from the incoming RF signal or as a frequency multiplier for clutter suppression purposes.[1,2] However, to be suitable for such IoT applications, a list of requirements needs to be fulfilled by the device. (1) The price point and (2) the often desired mechanical flexibility require cost-effective production, involving a printing process on low temperature substrates, typically based on polymers or paper. (3) Further,

This is an open access article under the terms of the Creative Commons Attribution License, which permits use, distribution and reproduction in any medium, provided the original work is properly cited.
© 2020 The Authors. *Nano Select* published by Wiley-VCH GmbH

the performance of today's printable, flexible electronics needs improvement, as it is often limited by the moderate electronic performance accessible with current semiconductor functional inks. These inks are mainly based on metal oxides or organic materials. The advantage of organic materials is their high compatibility with solution process- and printability. Further, these materials do not require high processing temperatures, making their processing suitable for the usage of flexible and lightweight substrates.[3,4] Yet, the low charge carrier mobility in thin films of such materials limits the operational frequencies of printed state-of-the-art organic devices, such as diodes, to approximately 10 MHz.[5] The use of metal oxides, for example, diode implementation allows much higher switching speeds; however, the fabrication process has a tremendous impact on the final electronic performance. While manufacturing processes such as physical vapor deposition, pulsed laser deposition, and atomic layer deposition allow high device switching speeds in the GHz range, printing processes result in grain boundaries and a low thin film uniformity, which affects the device performance and has limited the application of printed metal oxides in large scale fabrication.[3,4] An approach to overcome these issues for printed UHF electronics and to combine solution processing with high frequency device operation is the use of silicon (Si) and to make it printable. One strategy to realize this idea is the fabrication of silane-based inks as a precursor to form high purity amorphous or micro-/nanocrystalline Si layers.[6] However, the pyrolytic transformation of silane requires high temperatures which are not suitable for most flexible substrates. Additionally, toxic monosilane is produced during the transformation and an inert atmosphere is needed because of the pyrophoric nature of liquid silanes.[4,7] Another concept was demonstrated by Sani et al., where particles pressed into a SU-8 matrix were used for a Schottky diode application operating up to cut-off frequencies of 1.8 GHz.[8,9] Yet, despite the good performance of this approach in terms of device switchability, the concept has performance limiting issues due to grain/particle boundaries, or due to the use of a multi-material particle system. Therefore, in the following, a printable Si diode technology approach is discussed, which is based on using Si-nanoparticle (Si-NP) inks with a cost below 10 micro $-Cent per diode, although high purity Si is used. These inks allow full control in terms of particle doping, printability, and substrate wettability. Grain/particle boundary issues are solved by a laser treatment of the deposited Si nanoparticles, which results into a self-organized cone-shaped μ-structure. Due to the lateral discontinuity of the μ-cones, as well as their small footprint, this structure is expected to be mechanically flexible. Additionally, this Si μ-structure is highly crystalline as demonstrated in Section 2, and therefore offers great potential for high frequency applications. Embedded into an insulator matrix, these μ-cones are used for the realization of a new type of Schottky diode working up to 2.84 GHz.

2 | RESULTS AND DISCUSSION

For the device processing, Si-NPs synthesized in a hot-wall reactor are used. For a detailed process and device fabrication description see Section 3. A brief device process overview is discussed in the following. In order to allow for solution processing, the NPs are dispersed and electrostatically stabilized in ethanol. The ink is spin-coated on top of a sputter-deposited tungsten (W) layer forming a porous Si layer (Figure 1A). A pulsed laser treatment of the ~450 nm thick NP film with a KrF excimer laser emitting at 248 nm with 2.07 J cm^{-2} leads to an initial melting. Subsequently, the Si surface tension in conjunction with the large density of heterogeneities of the Si nanoparticle thin film will cause the Si melt to agglomerate/dewett in random locations, forming the porous nanosphere network shown in Figure 1B.[10,11] The resulting μ-cones have slightly different shapes and heights, as can be seen in Figures 1B and 2B, which is the consequence of the cone density being controlled by the laser energy density and the cone height dependence on the Si-NP layer thickness. To form a Schottky diode structure, the Si μ-cones are embedded in SU-8 serving as an insulator to ensure the current flow through the silicon and to avoid shortening the device. A layer of 200 nm aluminum is evaporated as a top contact metallization. A scanning electron microscope image of a diode integrated μ-cone is shown in Figure 2A. The device area is defined by the size of the circular top contact, which equals 0.78 mm^2 and includes the active area defined by the area covered with Si μ-cones and the parasitic capacitance caused by the insulator between the cones. With a cone density of approximately 600,000 cones per mm^2, this translates into roughly 468,000 single cone diodes in parallel per device. To examine the influence of the NP doping concentration on the current-voltage (IV) behavior of the μ-cone diodes, differently doped nanoparticles are used for the diode realization. For type I samples intrinsic particles are used, type II samples are realized using Si-NPs with a doping concentration of 5×10^{16} cm^{-3} and finally for type III samples a NP doping concentration of 5×10^{17} cm^{-3} is used.

Before the electronic functionality of the Si μ-cone diodes is evaluated, an investigation of the cone crystallinity using μ-Raman spectroscopy is discussed in the following. Here, a spot diameter of ~1 µm allows for the measurement of individual μ-cones. Raman spectra of a representative nanoparticle thin film, laser processed

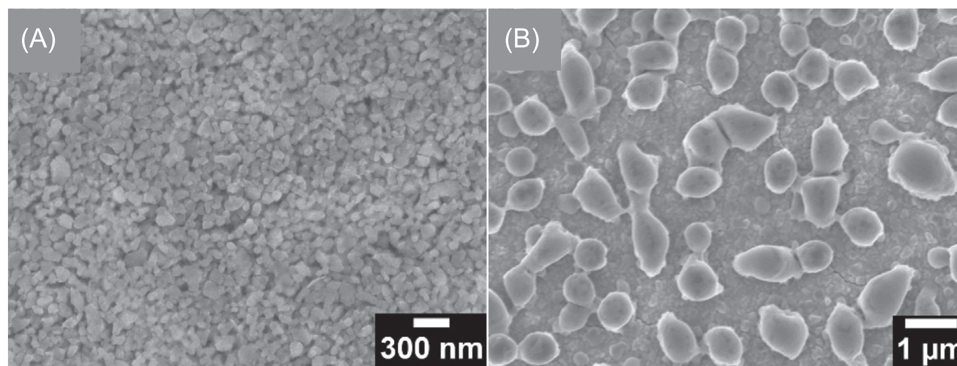

FIGURE 1 Scanning electron microscope (SEM) image of (A) a Si-NP thin film and (B) the self-organized cone shaped Si structure caused by the laser treatment of the Si-NP thin film laser modified with an effective laser energy density of 2.07 J cm^{-2}.

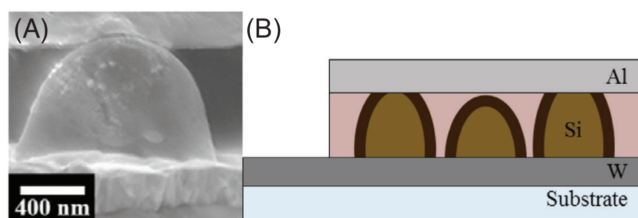

FIGURE 2 Crosscut images of the resulting μ-cone diode structure. (A) SEM image of one Si μ-cone embedded in an insulator and sandwiched between W as bottom and Al as top contact metallization. (B) Schematic image of the diode structure displaying the varying cone heights.

μ-cones, as well as a single crystalline Si reference are illustrated in Figure 3. For comparison, these are normalized to the maximum of the Raman peak centered at ~520 cm^{-1}. Further, a Raman intensity offset is used for clarity. The Raman spectrum of the unsintered NPs (a) in Figure 3 can be considered as a mix of crystalline and amorphous Si-fractions. The peak centered at 520 cm^{-1} corresponds to the transverse optical (TO) phonon energy of crystalline Si (c-Si). Compared to the c-Si reference (c), this peak position is slightly shifted towards lower energies ($\Delta\omega = 1.8$ cm^{-1}), which is due to the small particle size d < 70 nm.[12,13] The asymmetrical broadening towards lower energies can be attributed to the TO phonon peak of amorphous Si (underlaying broad peak at ~480 cm^{-1}). This broad peak and the lower energy peaks (inset Figure 3) are caused by the amorphous-like components of the sample, including grain boundaries and surfaces which can be considered as disordered material.[14] However, after the laser modification and Si µ-cone formation, the structure yields a highly crystalline signal, as can be seen from spectrum (b) in Figure 3, with a sharp Raman peak centered at 521.6 cm^{-1}. This is in good agreement with the Raman signal of the monocrystalline Si-reference (c). The crystalline volume fraction of the μ-cones is considered to be 100%, as no TO

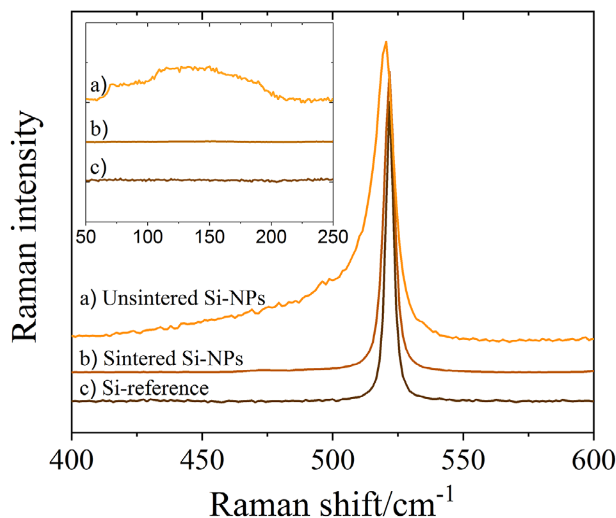

FIGURE 3 First order Raman spectra of the unsintered Si-NPs (a) and the Si μ-cone structures (sintered Si-NPs) (b) compared to a c-Si reference (c). For comparison, these are normalized to the maximum of the Raman peak centered at ~520 cm^{-1}. Further, a Raman intensity offset is used for clarity. Inset: Lower energy peaks attributed to amorphous-like components.

phonon modes of amorphous Si and no lower energy peaks (inset Figure 3) are detected. The slightly increased Full Width Half Maximum (FWHM) of the Raman main peak of the Si μ-cones, when compared to the c-Si reference (4.77 and 3.50 cm^{-1}) can be attributed to existing internal strain and grain size effects.[15]

In the following, the electronic functionality of the Si μ-cone diodes is discussed. Due to their slightly different shape and height, as outlined in conjunction with Figures 1 and 2, each μ-cone has a different contribution to the current flow. Therefore, the current flow is not homogeneously distributed over the whole contact area and consequently, rather than using the current density, it is more appropriate to describe the charge transport through the device using absolute current levels.

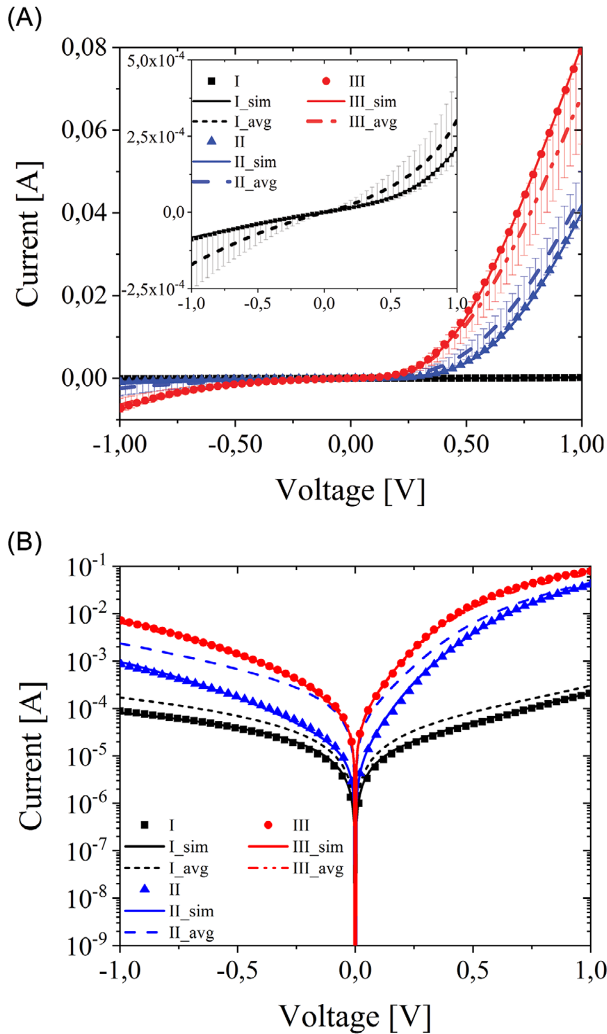

FIGURE 4 (A) Linear scaled plot of the average current values for the different sample types I-III (dashed lines) and the related standard deviation based on three (I) or four samples (II and III). Furthermore, one measured IV-curve per doping concentration (bold scatter plot) is modeled with the thermionic emission (TE) and thermionic field emission (TFE) theory based simulation. Inset in (A): Close-up view of the IV-curve of sample I to show its rectification at a smaller scale. (B) Semi-logarithmic plot of the average IV-characteristics, as well as one respective modeled device characteristic.

Average IV-characteristics and their standard deviation for devices using the three doping levels under investigation are shown in Figure 4 (dashed lines and error bars). All diodes exhibit a clear rectifying behavior and an increase in doping concentration leads to larger currents. In comparison to the intrinsic samples (dashed line inset Figure 4), an increased doping concentration of 5×10^{17} cm^{-3} (red dashed line) leads to a current enhancement by two orders of magnitude for voltages greater than 0.25 V. The reverse current follows the same trend as can be seen from Figure 4B. Further, the turn-on as well as the break-down voltages are shifted towards lower values, and the current slope increases for larger doping concentrations at higher voltage values. This is suggested to be the consequence of a decrease in series resistance and therefore an increase in the semiconductor bulk conductivity.[16,17] Unlike the IV-characteristic of a standard Si diode, the curve progression of the samples seems to be smoother and deviates from the expected steep exponential increase. Further, the reverse current is relatively high, which significantly reduces the On/Off-ratio of the devices (On/Off ratio < 50 in the considered range).

In the following, this new type of Schottky diode is described using thermionic emission (TE) and thermionic field emission (TFE) theory with a large signal model.[17,18] Aside from the non-linearity of the current, the model considers barrier lowering and the diode junction capacitance. Exemplarily one arbitrary device per doping concentration was modeled. These devices are highlighted in Figure 4 by the bold scatter plots. The simulation results (solid lines) are in good agreement with the measured data and are within the standard deviation of the respective device. Here, only a brief overview of the device model is given. Further information can be found in recent contributions.[19–21]

The current-voltage relationship of a diode with a single Si μ-cone can be described as follows:

$$I = I_S \exp\left(\frac{V - IR_S}{E_0}\right)\left[1 - \exp\left(-\frac{V - IR_S}{V_{th}}\right)\right] \quad (1)$$

where V represents the applied voltage in the forward direction and R_S the series resistance, which considers the Si-bulk resistance as well as the contact resistance of the ohmic contact. The parameter E_0 (see Equation (2)) is used to relate the tunneling energy E_{00} and the thermal voltage V_{th} assuming room temperature ($T = 300$ K).

$$E_0 = E_{00} \coth\left(\frac{E_{00}}{V_{th}}\right). \quad (2)$$

The tunneling energy E_{00} (see Equation (3)) is mainly dependent on the doping concentration N_A and the effective mass of the majority carriers m^*, as well as the semiconductor permittivity ε_r:

$$E_{00} = 18.5 \cdot 10^{-15} \sqrt{\frac{N_A}{m^* \epsilon_r}}. \quad (3)$$

The saturation current I_S is dependent on the applied theory. For TE it equals:

$$I_{S,TE} = AA^* T^2 \exp\left(\frac{-\phi_b}{V_{th}}\right) \quad (4)$$

And for TFE:

$$I_{S,TFE} = AA^*T^2\exp\left(\frac{-\xi}{V_{th}}\right)\frac{\sqrt{\pi E_{00}(\phi_b - V - \xi)}}{V_{th}\cosh\left(\frac{E_{00}}{V_{th}}\right)}\exp\left(\frac{-\phi_b + \xi}{E_0}\right) \quad (5)$$

with A being the effective diode area, A^* the effective Richardson constant which equals 32 $Acm^{-2}K^{-2}$ for p-type Si, ξ describes the difference between the Fermi energy and the valence band maximum. Further, ϕ_b corresponds to the Schottky barrier height. Due to the voltage dependency of the transition between pure TE and TFE, the following condition for TFE is used:[18]

$$\frac{\cosh^2\left(\frac{E_{00}}{V_{th}}\right)}{\sinh^3\left(\frac{E_{00}}{V_{th}}\right)} < \frac{2}{3}\frac{\phi_b - V}{E_{00}}. \quad (6)$$

As every individual μ-cone diode has a slightly different shape and size, as discussed above, their embedding varies. Higher cones stand out from the insulator layer, whereas others are still covered with a thin insulating layer. Consequently, every μ-cone diode exhibits a different Schottky barrier height. Therefore, a parallel circuit of 1000 different elementary diodes is assumed for the modeling effort. Even though the real devices consist of approximately 468,000 parallel-connected μ-cone diodes, this sample size is sufficient to cover the underlying statistics. A more detailed account for the modeling of such parallel-connected μ-cone diodes can be found elsewhere.[19] The distribution of the barrier height from cone diode to cone diode is analyzed by utilizing a random barrier height for the individual elementary diodes, assuming a Gaussian distribution with the mean value $\overline{\phi_b}$ and the standard deviation σ. The resulting sample barrier heights for the different doping concentrations are $\overline{\phi_{b,I}} = 1.35$ eV and $\sigma_I = 0.4$ eV (intrinsic), $\overline{\phi_{b,II}} = 0.86$ eV and $\sigma_{II} = 0.21$ eV (p = $5{\cdot}10^{16}$ cm^{-3}), $\overline{\phi_{b,III}} = 0.7\, eV$ and $\sigma_{III} = 0.16\, eV$ (p = $5{\cdot}10^{17}$ cm^{-3}). These mean barrier heights are relatively high compared to literature values of standard Si devices,[17] which can be explained by the already addressed cone height variation (Figure 2B). Cones smaller than the thickness of the insulator exhibit a native oxide layer and are still embedded in the insulator (Figure 2B: middle μ-cone). These interlayers will most likely lead to an increase and variation in barrier height. Deviations towards lower barrier values are assumed to be the consequence of μ-cones not covered by the polymer. As the native oxide of these μ-cones has been removed by a hydrofluoric acid (HF) dip, it is suggested that these cones carry most of the current. Furthermore, this distribution in the single cone barrier height and the related unequal distribution in current flow are responsible for the discussed IV-characteristic deviation when compared to an ideal device. The series resistances determined by the simulation are $R_{S,I} = 660\ \Omega$, $R_{S,II} = 7.3\ \Omega$ and $R_{S,III} = 6\ \Omega$. As expected, an increase in doping concentration leads to a decreased series resistance.

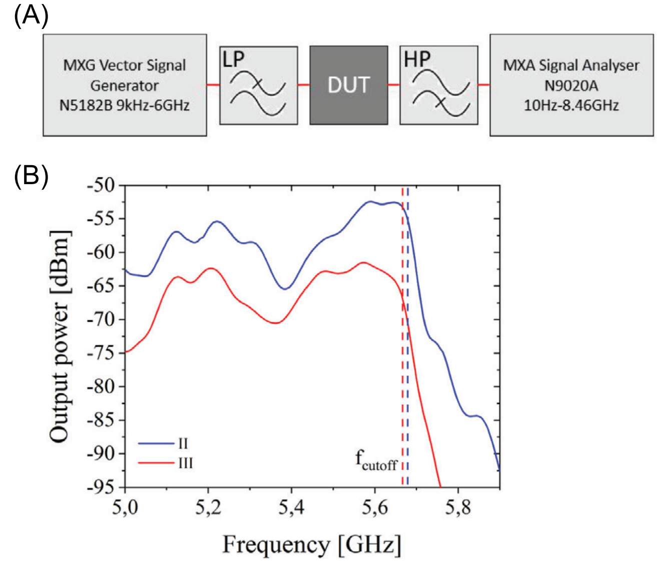

FIGURE 5 High frequency measurement. (A) Schematic representation of the measuring set-up consisting of a frequency generator and analyzer and two frequency filters. A low pass (LP) filter in front of the device under test (DUT) is used to suppress higher order harmonics of the generator. A high pass (HP) filter is used to avoid the generation of higher order harmonics inside the analyzer. (B) Measured output power of the generated second order harmonic under zero bias condition with 15 dBm input power. To get the excitation frequency the frequency value has to be halved.

The aim is to use the Si μ-cone diodes as frequency multipliers for clutter suppression purposes in low-cost, passive and chipless RFID tag applications. With this application in mind, the cutoff frequency of the devices is determined by measuring the second order harmonics, generated by the diodes due to their non-linearity under zero bias condition. For the measurements, a set-up consisting of a frequency generator and an analyzer in combination with two frequency filters is used (Figure 5A). A low pass (LP) filter is required to suppress higher order harmonics of the generator. A high pass (HP) filter is used to suppress the excitation frequency and therefore the generation of higher order harmonics inside the analyzer. For the investigation of the frequency response, a type II sample (p = 5×10^{16} cm^{-3}) and a type III sample (p = 5×10^{17} cm^{-3}) with reduced device areas of a few hundred μm^2 integrated into a microstrip line are used. The decrease in the active area is required for high frequency operation, as the value of the parasitic capacitance is directly related to the device area. Type I samples are not used in this experiment, as the

turn-on voltage is high and the determined high series resistance would lead to enhanced losses. The frequency dependent second order harmonic plot of the devices under test is illustrated in Figure 5B. Here, an output power of approximately −60 dBm for the type II sample and −66 dBm for the type III sample were detected up to a frequency of 5.66 GHz, when using an input power of 15 dBm. This value corresponds to an excitation frequency of 2.83 GHz. For higher frequencies, the signal starts to drop down to the noise level at −95 dBm. Considering the output power at 2.83 GHz as a reference, the −3 dB cutoff frequencies of these diode structures are estimated at $f_{cutoff,II}$ = 2.84 GHz (p = 5 × 10^{16} cm^{-3}) and $f_{cutoff,III}$ = 2.83 GHz (p = 5 × 10^{17} cm^{-3}). The output power variation at lower frequencies is attributed to the frequency-dependence of the reflection factor.[22,23] The observed high losses in this experiment are the consequence of a non-ideal impedance matching, as well as a relatively high series resistance (approximately a few kΩ). The latter is caused by the used top contact design, as well as process fluctuations regarding the top contact size. These effects superimpose the influence of the variation in doping concentration on the device frequency behavior. It would be excepted, that a higher doping concentration leads to a higher conductivity and therefore an increased device output power. However, this is not observed here. Nevertheless, ultra-high switching speeds are demonstrated for this new type of potentially printable Schottky device concept, by showing a bandwidth of up to 5.68 GHz when using the introduced Schottky diodes as a frequency doubler.

In summary, a new type of Si μ-cone based Schottky diode concept is introduced, which can be solution processed and still allows for operating frequencies up to 2.84 GHz. For the device processing, Si-NPs are electrostatically stabilized in ethanol to form solution processable inks. A laser treatment of the ink deposited thin films leads to a self-organized cone-shaped Si μ-structure, which is highly crystalline as demonstrated by Raman measurements. Embedded in an insulator and sandwiched between one ohmic and one Schottky contact, the concept allows to realize Schottky diodes. Their IV-characteristic can be described in good agreement by using the TE and TFE theory. When compared to ideal Si devices, the Si μ-cone Schottky diodes exhibit a smoother curve progression, higher leakage currents, and a reduced On/Off-ratio. This deviation can be attributed to a variation in single cone barrier height. In conclusion, a printable crystalline Si based device is demonstrated, which has allowed for an output bandwidth of 5.68 GHz when used as a frequency doubler. Thereby, the switching speed of the printable Si device concept extends well into the microwave range, putting flexible, low-cost, and high frequency electronics within reach.

3 | MATERIALS AND METHODS

The Si-NPs are synthesized in a hot-wall reactor (HWR). For Boron doping a mixture of the gaseous precursors monosilane and diborane is thermally decomposed within the HWR, whereas nitrogen serves as the carrier gas.[24,25] The diameter of the NPs is <70 nm.

To fabricate the ink, the NPs are dispersed in ethanol and milled using yttrium stabilized zirconia beads. Afterward, the dispersion consisting of 16 wt% Si-NPs is filtered with a glass fiber filter with a pore size of 0.7 µm and it is spin-coated on top of a sputter deposited tungsten layer.

The ∼450 nm thick NP thin film is modified using an ATLEX-300SI KrF excimer laser (ATL Lasertechnik GmbH), emitting at a wavelength of 248 nm with a pulse duration of 4–6 ns. The laser beam has a top-hat – Gaussian line profile of 10 mm x 29 µm (FWHM). The repetition frequency, the scan speed, and the effective energy density were set to 100 Hz, 9.3 mm min^{-1} and 2.07 J cm^{-2}. To avoid oxidation of the Si-melt during processing, the process chamber is flushed with nitrogen.

SU-8 2000.5 is used as an insulator between anode and cathode, and it is structured via photolithography. Plasma etching for 20 seconds is used to remove the SU-8 from the top of the cones.

Afterward, a hydrofluoric acid (HF) dip (5% HF, 20 seconds) is used to remove the native silicon oxide layer from the top of the cones and a layer of 200 nm aluminum is evaporated as top contact metallization. For the IV-measurements the top contact size equals 0.78 mm^2. The average current values are based on three devices for type I samples, and four devices for type II as well as type III samples. For the measurement of the second order harmonic the top contact size is reduced to a few hundred μm^2 (type II sample: 658 μm^2 and type III sample: 826 μm^2).

The Raman spectra of the silicon have been measured at room temperature using a Renishaw InVia Raman microscope in backscattering geometry (grating 2400 lines mm^{-1}) with a spot diameter of ∼1 µm. An excitation wavelength of 532 nm is used and the laser intensity is set to 78 µW.

DC measurements are conducted using a KEITHLEY 4200-SCS. For the microwave measurements, an excitation frequency sweep between 2.5 and 3 GHz with 15 dBm input power is generated using a Keysight MXG Vector Signal Generator N5182B. To suppress higher order harmonics of the generator, a low pass filter with a cut off frequency of 3 GHz is used in front of the

device. The second order harmonics are analyzed using a Keysight MXA Signal Analyzer N9020A. To avoid the generation of higher order harmonics inside the analyzer, a high pass filter with a cut off frequency of 3 GHz in front of the analyzer is used to suppress the excitation frequency.

ACKNOWLEDGMENTS

This work was supported by the German Research Foundation (DFG) as part of the project *Flexible Radio Frequency Identification Tags and Systems* (FlexID). Additionally, it was funded as part of the Interreg V project *Druckbare RFID-Tags für Massenmärkte* (DruIDe).

CONFLICT OF INTEREST

There are no conflicts of interest.

REFERENCES

1. P. Nintanavongsa, U. Muncuk, D. R. Lewis, K. R. Chowdhury, *IEEE J. Emerg. Sel. Topics Circuits Syst.* **2012**, *2*, 24.
2. H. Jabbar, Y. Song, T. Jeong, *IEEE Trans. Consumer Electron.* **2010**, *56*, 247.
3. J. Semple, D. G. Georgiadou, G. Wyatt-Moon, G. Gelinck, T. D. Anthopoulos, *Semicond. Sci. Technol.* **2017**, *32*, 123002.
4. Y. Chu, C. Qian, P. Chahal, C. Cao, *Adv. Sci.* **2019**, *206*, 1801653.
5. K. E. Lilja, T. G. Bäcklund, D. Lupo, T. Hassinen, T. Joutsenoja, *Organic Electronics* **2009**, *10*, 1011.
6. T. Shimoda, Y. Matsuki, M. Furusawa, T. Aoki, I. Yudasaka, H. Tanaka, H. Iwasawa, D. Wang, M. Miyasaka, Y. Takeuchi, *Nature* **2006**, *440*, 783.
7. S. Han, X. Dai, P. Loy, J. Lovaasen, J. Huether, J. M. Hoey, A. Wagner, J. Sandstrom, D. Bunzow, O. F. Swenson, I. S. Akhatov, D. L. Schulz, *J. Non Cryst. Solids* **2008**, *354*, 2623.
8. N. Sani, M. Robertsson, P. Cooper, X. Wang, M. Svensson, P. Andersson Ersman, P. Norberg, M. Nilsson, D. Nilsson, X. Liu, H. Hesselbom, L. Akesso, M. Fahlman, X. Crispin, I. Engquist, M. Berggren, G. Gustafsson, *Proc. Natl. Acad. Sci. USA* **2014**, *111*, 11943.
9. N. Sani, X. Wang, H. Granberg, P. Andersson Ersman, X. Crispin, P. Dyreklev, I. Engquist, G. Gustafsson, M. Berggren, *Sci. Rep.* **2016**, *6*, 28921.
10. M. Caninenberg, D. Kiesler, N. Benson, R. Schmechel, *Opt. Laser Technol.* **2017**, *90*, 33.
11. M. Caninenberg, E. Verheyen, D. Kiesler, B. Stoib, M. S. Brandt, N. Benson, R. Schmechel, *Opt. Laser Technol.* **2015**, *74*, 132.
12. C. Meier, S. Lüttjohann, V. G. Kravets, H. Nienhaus, A. Lorke, H. Wiggers, *Physica. E Low Dimens. Syst. Nanostruct.* **2006**, *32*, 155.
13. H. Richter, Z. P. Wang, L. Ley, *Solid State Commun.* **1981**, *39*, 625.
14. C. Smit, R. A. C. M. M. van Swaaij, H. Donker, A. M. H. N. Petit, W. M. M. Kessels, M. C. M. van de Sanden, *J. Appl. Phys.* **2003**, *94*, 3582.
15. C.-C. Kuo, *Opt. Lasers Eng.* **2009**, *47*, 612.
16. E. H. Rhoderick, *IEE Proc. I Solid State Electron. Devices UK* **1982**, *129*, 1.
17. S. M. Sze, K. K. Ng, *Physics of Semiconductor Devices*, Wiley-Interscience, Hoboken, NJ **2007**.
18. E. H. Rhoderick, R. H. Williams, *Metal-Semiconductor Contacts*, Claredon Press, Oxford **1988**.
19. K. Neumann, L. Kuhnel, F. Langer, A. Rennings, N. Benson, R. Schmechel, D. Erni, *IEEE Trans. Microwave Theory Techn*. **2020**, *68*(6), 2151.
20. K. Neumann, J. Moeller, L. Kuehnel, A. Rennings, N. Benson, R. Schmechel, D. Erni, Excerpt from the Proceedings of the 2018 COMSOL Conference in Lausa **2018**.
21. K. Neumann, L. Kühnel, F. Langer, A. Rennings, N. Benson, R. Schmechel, D. Erni, Analysis of stochastic Schottky barrier variations within printed high frequency rectifiers for harmonics generation. In *Presented at the IEEE MTT-S International Microwave Workshop Series on Advanced Materials and Processes (IMWS-AMP 2019)*, July 16–18, Bochum, Germany, Session TH2.2: 'Advanced Devices and Circuits', paper no. TH2.2-1, pp. 169-171, **2019**.
22. H. Heuermann, O. Mildenberger, *Hochfrequenztechnik*, Vieweg+Teubner Verlag, Wiesbaden **2005**.
23. D. M. Pozar, *Microwave Engineering*, Wiley, Hoboken **2012**.
24. H. Wiggers, R. Starke, P. Roth, *Chem. Eng. Technol.* **2001**, *24*, 261.
25. T. Hülser, S. M. Schnurre, H. Wiggers, C. Schulz, *KONA* **2011**, *29*, 191.

How to cite this article: Kühnel L, Neumann K, Neises J, et al. Nanoparticle ink-based silicon Schottky diodes operating up to 2.84 GHz. *Nano Select*. 2020;1:659–665.
https://doi.org/10.1002/nano.202000102